Pergamon

Int. J. Solids Structures Vol. 31, No. 6, pp. 823–833, 1994

0020–7683/94 $6.00 + .00

EFFECT OF *T*-STRESS ON MODE I CRACK GROWTH RESISTANCE IN A DUCTILE SOLID

V. TVERGAARD
Department of Solid Mechanics, The Technical University of Denmark, Building 404, DK-2800 Lyngby, Denmark

and

J. W. HUTCHINSON
Division of Applied Sciences, Harvard University, Cambridge, MA, U.S.A.

(*Received* 24 *May* 1993; *in revised form* 10 *September* 1993)

Abstract—An elastic–plastic crack growth model, with a traction–separation law specified on the crack plane to characterize the fracture process, is used to study the effect of the non-singular *T*-stress, acting parallel to the crack plane. The work of separation per unit area and the peak normal stress are the two main parameters used to characterize the fracture process, and crack growth resistance curves are calculated numerically for a number of values of the peak stress to initial yield stress ratio, and for different levels of strain hardening. Small-scale yielding in plane strain is considered with the remote field specified by a constant value of the *T*-stress, applied initially, and an increasing magnitude of the mode I stress intensity factor. It is shown that the predicted *T*-stress dependence of the fracture toughness during crack growth is qualitatively similar to experimental observations, even though the experiments go beyond small-scale yielding.

1. INTRODUCTION

The effect of crack-tip constraint on fracture toughness of ductile materials has attracted a great deal of interest recently. Thus, starting from conditions of small-scale yielding Betegon and Hancock (1991) and Du and Hancock (1991) have studied the effect of the non-singular stress term T, acting parallel to the crack plane, on elastic–plastic crack-tip fields. They found that J-dominance is maintained for zero or positive T-stresses, while negative T-stresses cause loss of J-dominance of the plastic crack-tip fields. The significant influence of the T-stress on the shape and size of the plastic zone which develops at the crack-tip has been demonstrated earlier by Larsson and Carlsson (1973) and Rice (1974). Hancock *et al.* (1991) have tested a wide range of through-cracked geometries of an ASTM 710 grade A steel and have correlated the geometry dependence of crack extension in plane strain with the crack-tip constraint as parameterized by the T-stress, with an approximate extension of that measure in fully plastic conditions. O'Dowd and Shih (1991, 1992) have studied a two-term expansion of the plastic crack-tip fields with the first term characterized by the applied J and with an amplitude Q of the second term. It is argued by O'Dowd and Shih (1992) that the J–Q approach is preferable under fully yielded conditions, where the T-stress is not so clearly defined.

For a ductile solid subject to mode I plane strain crack growth Tvergaard and Hutchinson (1992) have computed crack growth resistance curves to determine the effect of plastic dissipation on fracture toughness. In this study the fracture process is represented in terms of a traction–separation law in which the primary parameters are the work of separation per unit area, Γ_0, and the peak traction, $\hat{\sigma}$. In the absence of plasticity the value of the stress intensity factor needed to advance the crack corresponds directly to the work of fracture per unit area, Γ_0, but the computations show that a plastic zone moving with the crack-tip can increase the fracture toughness by a significant factor, dependent mainly on the peak traction to initial yield stress ratio, $\hat{\sigma}/\sigma_Y$, and the strain hardening exponent, N. The model describes the role of plasticity for the interface toughness of similar materials bonded together, but is also relevant to studies of crack growth in a homogeneous material by various failure mechanisms, including void growth and coalescence in a certain range

of parameters. A similar cohesive zone model has been used by Tvergaard and Hutchinson (1993) to analyse the mixed mode toughness for a crack growing along an interface joining an elastic–plastic solid to a solid which does not yield plastically. Both these studies focus on small-scale yielding in plane strain with the remote elastic field specified by the mode I stress intensity factor or the magnitude and phase of the mixed mode stress intensity factors.

In the present paper the results for mode I crack growth resistance in a homogeneous material (Tvergaard and Hutchinson, 1992) are extended to account for the effect of a non-zero T-stress. The cohesive zone model is identical to that used in our previous study, and the assumption of small-scale yielding is maintained. The predicted T-stress dependence of the fracture toughness during crack growth is qualitatively similar to the dependence observed experimentally, especially in the careful study of Hancock *et al.* (1991). For reasons discussed at length at the end of the paper, no attempt has been made to accurately simulate the material these authors tested.

2. PROBLEM FORMULATION

In the case of an elastic solid the Griffith criterion for crack growth is $\mathscr{G} = \Gamma_0$, where $\mathscr{G}$ is the energy release rate as calculated for a line crack using elasticity theory and Γ_0 is the work of separation per unit area required to create the two crack surfaces. However, when plastic yielding takes place around the crack-tip, the crack growth resistance, $\Gamma_R(\Delta a)$, exceeds Γ_0 and grows with increasing crack extension Δa until a steady-state value Γ_R^{ss} is reached. For small-scale yielding in plane strain mode I the critical value of the energy release rate may be expressed in terms of the stress intensity factor K, so that the resistance curve takes the form

$$K = K_R(\Delta a), \tag{1}$$

where $K_R = [E\Gamma_R/(1-\nu^2)]^{1/2}$, ν is Poisson's ratio, and E is Young's modulus. Such resistance curves for a homogeneous elastic–plastic material were calculated by Tvergaard and Hutchinson (1992) based on a cohesive zone representation of the fracture process. The same cohesive zone and elastic–plastic material formulations are used in the present analyses.

The traction–separation relation used to model the fracture process is shown in Fig. 1. The work of separation per unit area is:

$$\Gamma_0 = \int_0^{\delta_c} \sigma \, \mathrm{d}\delta = \tfrac{1}{2}\hat{\sigma}[\delta_c + \delta_2 - \delta_1]. \tag{2}$$

This separation law is fully specified by Γ_0, $\hat{\sigma}$, δ_1/δ_c and δ_2/δ_c, where the latter two parameters are shape parameters.

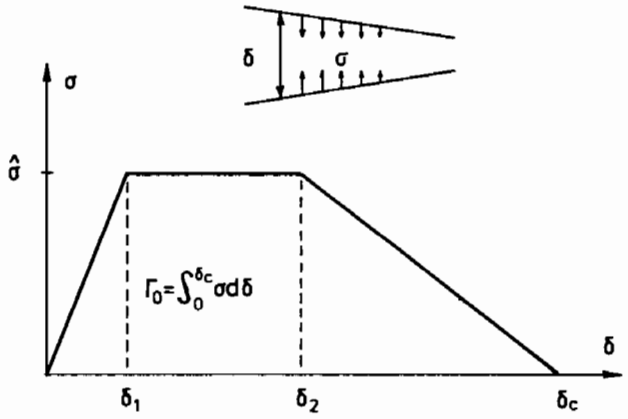

Fig. 1. Traction–separation relation for fracture process.

The elastic–plastic solid has an initial tensile yield stress, σ_Y, and a true stress–logarithmic strain curve in uniaxial tension specified by

$$\varepsilon = \begin{cases} \sigma/E, & \text{for } \sigma \leqslant \sigma_Y \\ (\sigma_Y/E)(\sigma/\sigma_Y)^{1/N}, & \text{for } \sigma \geqslant \sigma_Y. \end{cases} \tag{3}$$

The tensile behaviour is generalized to multiaxial stress states assuming isotropic hardening and using the von Mises yield surface. Thus, the continuum behaviour of the solid is characterized by the set of parameters E, ν, σ_Y and N.

Finite strains are accounted for in the analysis, using a convected coordinate, Lagrangian formulation of the field equations, in which g_{ij} and G_{ij} are metric tensors in the reference configuration and the current configuration, respectively, with determinants g and G, and $\eta_{ij} = \frac{1}{2}(G_{ij} - g_{ij})$ is the Lagrangian strain tensor. The contravariant components τ^{ij} of the Kirchhoff stress tensor on the current base vectors are related to the components of the Cauchy stress tensor σ^{ij} by $\tau^{ij} = \sqrt{G/g}\sigma^{ij}$. Then, in the finite-strain generalization of J_2-flow theory discussed by Hutchinson (1973), the incremental stress–strain relationship is of the form $\dot{\tau}^{ij} = L^{ijkl}\dot{\eta}_{kl}$, with the tensor of instantaneous moduli given by

$$L^{ijkl} = \frac{E}{1+\nu}\left[\frac{1}{2}(G^{ik}G^{jl} + G^{il}G^{jk}) + \frac{\nu}{1-2\nu}G^{ij}G^{kl} - \beta\frac{3}{2}\frac{E/E_t - 1}{E/E_t - (1-2\nu)/3}\frac{s^{ij}s^{kl}}{\sigma_e^2}\right] - \frac{1}{2}(G^{ik}\tau^{jl} + G^{jk}\tau^{il} + G^{il}\tau^{jk} + G^{jl}\tau^{ik}). \tag{4}$$

Here, the effective von Mises stress is $\sigma_e = (3s_{ij}s^{ij}/2)^{1/2}$, $s^{ij} = \tau^{ij} - G^{ij}\tau^k_k/3$ is the stress deviator, and the value of β is 1 or 0 for plastic yielding or elastic unloading, respectively. Furthermore, E_t is the slope of the true stress vs natural strain curve (3) at the stress level σ_e.

The plane strain mode I crack growth analyses are carried out for conditions of small-scale yielding. Due to symmetry about the crack plane only half of the solid needs to be analysed, and the numerical computations are carried out for a semicircular region with initial radius A_0, as shown in Fig. 2. The x^1-axis is in the crack plane and the initial crack-tip is located at $x^1 = x^2 = 0$. The traction–separation relation used to model the fracture process (see Fig. 1) is specified everywhere on the boundary $x^1 > 0$, $x^2 = 0$ of the region analysed, while zero tractions are specified for $x^1 \leqslant 0$, $x^2 = 0$. It is noted that the stress σ used in the traction–separation relation (Fig. 1) is defined as a true stress. This is important in cases where crack-tip blunting starts to occur; but in most of the present computations the strains remain rather small, so that applying true stresses or nominal stresses in the traction–separation relationship would not make a great deal of difference.

According to the small strain linear elastic solution the in-plane stress components near the crack-tip are of the form

$$\sigma_{\alpha\beta} = \frac{K}{\sqrt{2\pi r}} f_{\alpha\beta}(\theta) + T\delta_{1\alpha}\delta_{1\beta}, \tag{5}$$

where (r, θ) are polar coordinates and δ_{ij} is Kronecker's delta. For mode I loading, K is the amplitude of the singular stress field, while T is a non-singular stress term, acting parallel to the crack plane. In the present analyses the T-stress is applied first, together with the corresponding transverse stress $\sigma_{33} = \nu T$ under plane strain conditions. Subsequently, additional displacements are specified on the outer semicircular boundary according to the singular K-field solution around the crack-tip. Thus, the uniform T-stress field applied initially is below the yield limit, and the additional loading is applied by incrementally increasing the amplitude K for the displacements on the semicircular boundary. At some stages of the deformation the value of the J-integral is calculated on a number of contours around the crack-tip to check agreement with the prescribed amplitude K of the edge

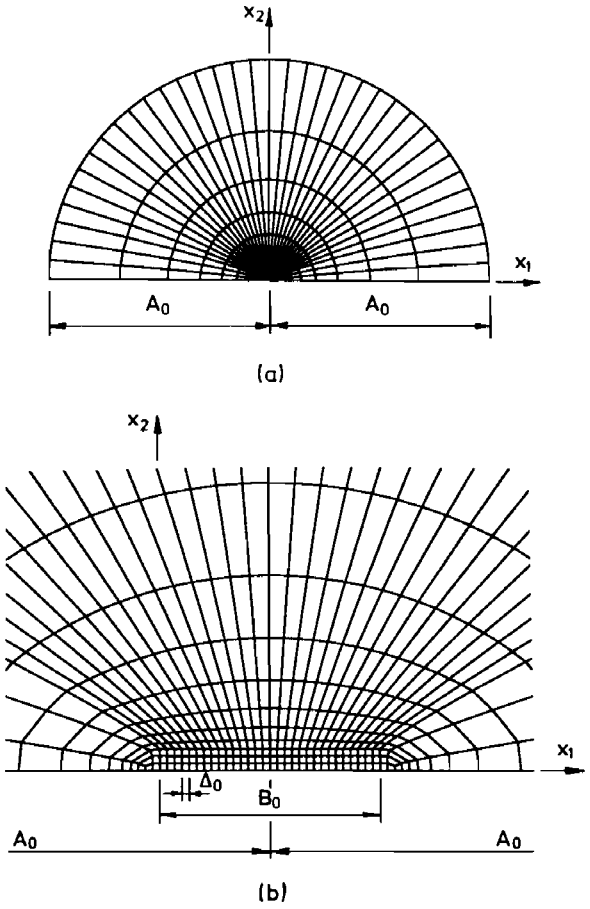

Fig. 2. Finite element mesh. (a) Full mesh. (b) Refined mesh along the crack line.

displacements. Very good agreement is found in the present computations, as long as the radius A_0 is chosen to be large enough. The independence of J on the value of T has been ensured by choosing this large outer radius.

The numerical analyses follow the scheme discussed in more detail by Tvergaard and Hutchinson (1992). Approximate solutions are obtained by a linear incremental method using a finite element approximation of the displacement fields in the incremental version of the principle of virtual work. The elements used are quadrilaterals each built-up of four triangular, linear-displacement elements. An example of the mesh used for the computations is shown in Fig. 2, where it is seen that a uniform mesh region with initial length B_0 in front of the initial crack-tip is used to model crack growth. A special Rayleigh–Ritz finite element method is used to control nodal displacements at the interface within the fracture process zone [see also Tvergaard (1990)] as is necesary when K has reached the steady-state value while the crack still grows.

In the uniform mesh region of length B_0 in front of the initial crack-tip the length of one square element is denoted as Δ_0. The present computations are carried out with $\delta_c = 0.1\Delta_0$, $\delta_1/\delta_c = 0.15$ and $\delta_2/\delta_c = 0.5$. The mesh shown in Fig. 2 corresponds to using $B_0 = 30\Delta_0$ and $A_0 = 2000\Delta_0$; but most of the computations have been carried out using a larger mesh with $B_0 = 60\Delta_0$ and $A_0 = 40.000\Delta_0$, for the same mesh size Δ_0.

Two reference quantities K_0 and R_0 are introduced for the presentation of the results

$$K_0 = [E\Gamma_0/(1-\nu^2)]^{1/2} \tag{6}$$

$$R_0 = \frac{1}{3\pi}\left(\frac{K_0}{\sigma_Y}\right)^2 = \frac{1}{3\pi}\frac{E\Gamma_0}{(1-\nu^2)\sigma_Y^2}. \tag{7}$$

Here, K_0 represents the mode I stress intensity factor needed to advance the crack when plastic dissipation is negligible, i.e. the stress intensity factor needed to supply just the work of the fracture process Γ_0. The reference length R_0 scales with the size of the plastic zone when $K \cong K_0$. In plane strain small-scale yielding $(K/\sigma_Y)^2/(3\pi)$ is commonly used to estimate the size of the plastic zone.

3. RESULTS

The values of the parameters specifying the elastic–plastic material behaviour are taken to be $N = 0.1$, $\sigma_Y/E = 0.003$ and $\nu = 0.3$ in most of the computations. The shape parameters for the traction–separation relation are taken to be $\delta_1/\delta_c = 0.15$ and $\delta_2/\delta_c = 0.5$, while the remaining two parameters Γ_0 (or K_0) and $\hat{\sigma}$ appear directly in the figures used to present the predictions of the model.

For the same set of material parameters, in the absence of T-stress ($T/\sigma_Y = 0$), it was found by Tvergaard and Hutchinson (1992) that plasticity gives essentially no contribution to the total work of fracture if the value of $\hat{\sigma}/\sigma_Y$ is less than 2. For $\hat{\sigma}/\sigma_Y$ larger than 2 the effect of plasticity starts to be noticeable, and it was found that increasing the steady-state work of fracture by a factor larger than 4 ($K^{ss}/K_0 > 2$) requires $\hat{\sigma}/\sigma_Y = 3.4$.

Figure 3 shows a number of crack growth resistance curves computed for a negative value of the T-stress, $T/\sigma_Y = -1$. Here, the crack growth resistance, $K_R(\Delta a)$, is normalized by K_0, and the crack extension is normalized by R_0. It is seen that according to the model applied here crack growth initates at $K = K_0$ in each case, as was also found in the absence of T-stress (Tvergaard and Hutchinson, 1992). The resistance K_R increases rapidly in the initial stage of crack growth and then more slowly in a comparatively large interval of $\Delta a/R_0$, until the peak is reached. In fact, for $\hat{\sigma}/\sigma_Y = 0.9$, where the plastic zone is small, the peak resistance is reached well beyond the maximum crack extension, $\Delta a/R_0 = 16$, shown in Fig. 3. The most important difference between the resistance curves found in the absence of T-stress and those in Fig. 3 for negative T-stress is that, even at values of $\hat{\sigma}/\sigma_Y$ much smaller than 2, the curves in Fig. 3 show a significant contribution of plasticity to the crack growth resistance.

In Fig. 4 crack growth resistance curves are shown for a fixed value, $\hat{\sigma}/\sigma_Y = 2.4$, of the peak stress in the traction–separation relation (2), but for different values of the T-stress. It is seen in Fig. 4 that plasticity essentially has no effect for $T/\sigma_Y = 0$; but a negative T-stress increases the size of the plastic zone and thus also the contribution of plasticity to the crack growth resistance. As in Fig. 3, crack growth initiates at $K = K_0$, and the resistance curves increase steeply during the first part of crack growth, while $\Delta a/R_0 < 0.2$. The value

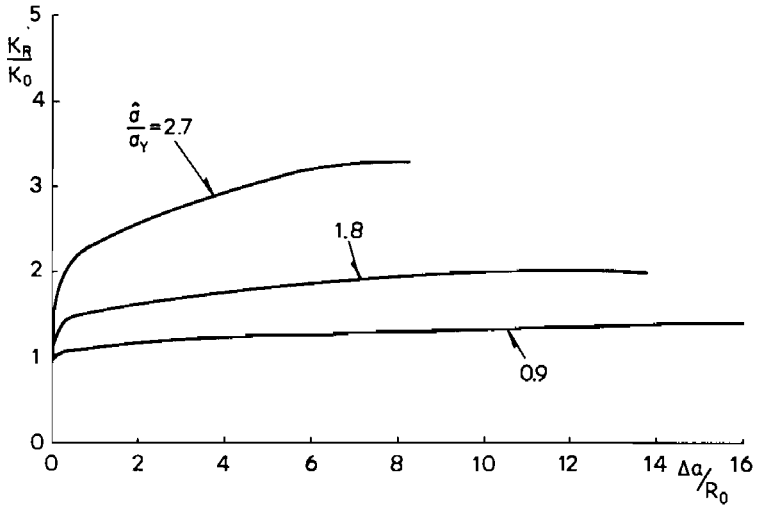

Fig. 3. Crack growth resistance curves for $T/\sigma_Y = -1$, $\sigma_Y/E = 0.003$ and $N = 0.1$.

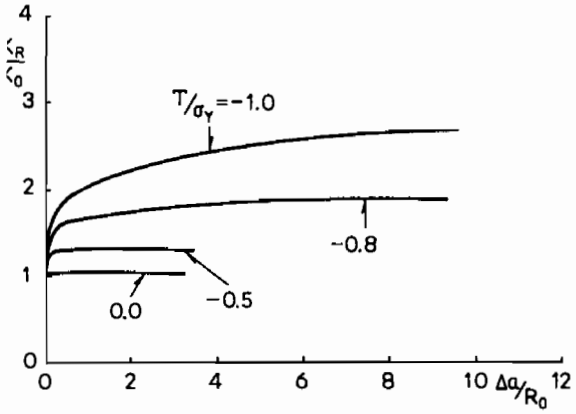

Fig. 4. Crack growth resistance curves for $\hat{\sigma}/\sigma_Y = 2.4$, $\sigma_Y/E = 0.003$ and $N = 0.1$.

of the reference length R_0 is the same for all four curves in Fig. 4, and it is seen that the amount of crack extension needed to reach the peak crack growth resistance is larger the larger the effect of plasticity.

It is noted that in a real cracked specimen the values of K and T will increase simultaneously, whereas in the present computations T is applied first and then kept constant. However, this is not expected to make any difference at all in the T-dependence of the steady-state toughness, since the ratio of T and K is fixed incrementally at this limit. There may be a small effect on the rising part of the R-curve, but the J-argument about initiation of crack growth at $K = K_0$ is unaffected.

The limiting value of K_R attained as the crack grows and approaches a steady-state is denoted as K^{ss}. Such limiting values are computed here as the peak values of resistance curves such as those shown in Figs 3 and 4. Results based on many computations of this type are plotted in Fig. 5 for different values of the T-stress, as functions of the peak stress $\hat{\sigma}$ in the traction–separation relation used to model the fracture process. The curve for $T/\sigma_Y = 0$ was also shown by Tvergaard and Hutchinson (1992). It is seen in Fig. 5 that the curve for $T/\sigma_Y = 0.5$ differs very little from that corresponding to zero T-stress, whereas the curves for negative values of the T-stress differ significantly. Thus, as also noted in relation to Fig. 3, a negative T-stress allows for a significant effect of plasticity on K^{ss}/K_0, at values of $\hat{\sigma}/\sigma_Y$ far below the limit value of 2 determined in the absence of T-stress.

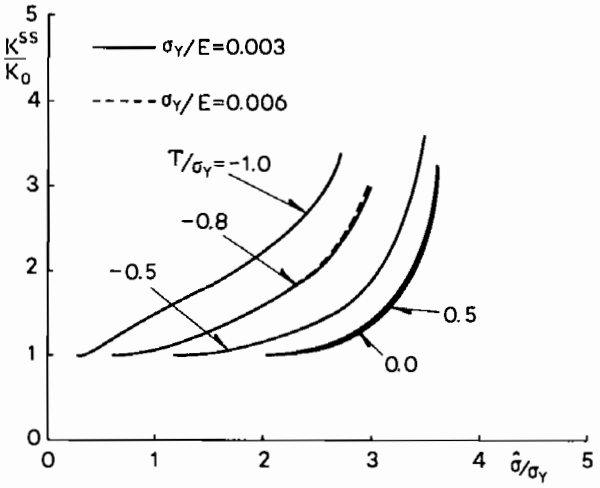

Fig. 5. Steady-state toughness as a function of $\hat{\sigma}/\sigma_Y$, for $N = 0.1$ and for five levels of the T-stress.

The sensitivity to changes in the material parameters is investigated by some additional computations. Thus, for $T/\sigma_Y = -0.8$ results for $\sigma_Y/E = 0.006$ are compared with those for $\sigma_Y/E = 0.003$ in Fig. 5. This comparison shows that the results in Fig. 5 are rather insensitive to the value of σ_Y/E, as was also found by Tvergaard and Hutchinson (1992) for $T = 0$. It is noted that in the computations for $\sigma_Y/E = 0.006$ the mesh size Δ_0 has been chosen so that the ratio Δ_0/R_0 is unchanged, to ensure the same numerical resolution relative to the plastic zone size.

The effect of a higher strain hardening level is shown in Fig. 6 by results for $N = 0.2$ and $\sigma_Y/E = 0.003$. Here, curves of K^{ss}/K_0 vs $\hat{\sigma}/\sigma_Y$ are shown for three values of the T-stress. It is seen that the curves for $T = 0$ and $T/\sigma_Y = 1$ differ rather little, whereas the curve for $T/\sigma_Y = -1$ shows a much higher steady-state fracture toughness at the same value of $\hat{\sigma}/\sigma_Y$. Comparing with Fig. 5, it is seen that for otherwise identical material parameters the increased strain hardening lowers the fracture toughness at all values of T/σ_Y. The higher strain hardening increases the tractions ahead of the tip and makes it easier to attain the peak stress $\hat{\sigma}$.

It is clear from previous investigations (Betegon and Hancock, 1991; Du and Hancock, 1991; O'Dowd and Shih, 1991, 1992) that in a high constraint situation, for positive T-stress, the near-tip stress and strain fields are characterized by the *HRR*-fields, whereas for negative T-stress there is a breakdown of J-dominance (i.e. the *HRR* stress levels ahead of the tip are not attained). It has been shown by these authors that in the high constraint situation the tensile stresses across the crack line in front of the crack-tip are high, approximately following the *HRR*-field prediction. However, as the crack-tip constraint is reduced, for increasing negative T-stress, the tensile stress level in front of the crack-tip gradually decays below the level predicted by the *HRR*-field. Now, in the present paper the tensile stress level in front of the crack-tip is very important, since it has been found for $T = 0$ (Tvergaard and Hutchinson, 1992) that the limiting fracture toughness is highly sensitive to the value of the peak stress $\hat{\sigma}$ in the traction–separation relation used to model the fracture process. Thus, when the tensile stress level in front of the crack-tip decays for a fixed value of $\hat{\sigma}$, an increased fracture toughness would be expected, and this is exactly the result found in Figs 5 and 6. In addition, the size of the plastic zone is larger for a negative T-stress at a given level of K, and this will also tend to increase the contribution of plastic dissipation to the steady-state fracture toughness.

Hancock *et al.* (1991) have carried out a series of experiments for an ASTM 710 grade A steel, using edge cracked bars, compact tension specimens and centre-cracked panels with various values of the crack length to specimen width ratio, a/W. These different specimen geometries give rise to a wide range of T-stress levels, and thus the test results show the effect of crack-tip constraint on the fracture toughness. For all specimens the measured J

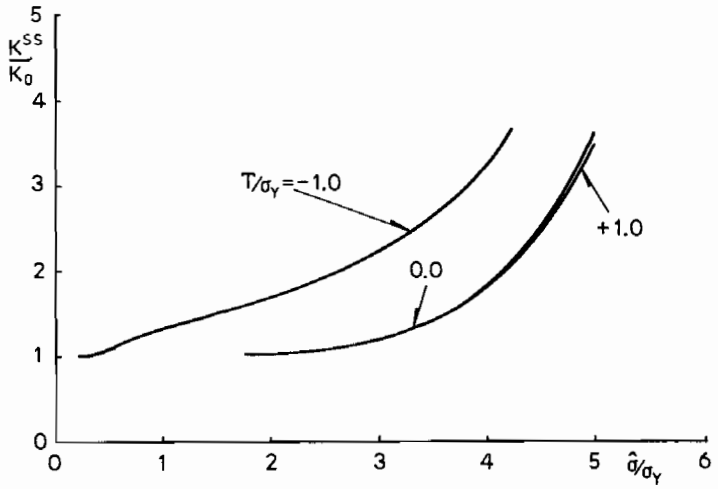

Fig. 6. Steady-state toughness as a function of $\hat{\sigma}/\sigma_Y$, for $N = 0.2$ and for three levels of the T-stress.

values are given for $\Delta a = 0$ (back extrapolation of the resistance curve), for $\Delta a = 200\ \mu$m and for $\Delta a = 400\ \mu$m. For $\Delta a = 0$, the measured J values show essentially no sensitivity to the value of the T-stress; but after some crack extension the measured J values show significant T-stress dependence, so that the fracture toughness increases with increasing negative value of the T-stress.

The material represented in the present computations is not directly comparable with that tested by Hancock *et al.* (1991); but it is noted that qualitatively the present model results show trends similar to those found in the experiments. Figure 4 represents resistance curves for a given material (fixed material and fracture parameters) subject to four different values of T-stress, and it is seen that the values of K_R predicted for $\Delta a = 0$ are identical, whereas after some crack extension the values of K_R are significantly higher for large negative T-stress. The material considered in Fig. 4 is special in that K_R/K_0 remains near unity for $T = 0$; but, even though the curves are not continued to large values of K^{ss}/K_0, Fig. 5 indicates that the trends will be similar for a higher value of the peak stress $\hat{\sigma}$ in the fracture process. Thus, for example, for $\hat{\sigma}/\sigma_Y = 3.4$, the predicted resistance curves still show $K_R/K_0 = 1$ at $\Delta a = 0$, and all curves show a significant increase of K_R/K_0 for increasing Δa, but clearly the increase is greater the larger the negative T-stress. In comparison, the experiments of Hancock *et al.* (1991) show that from $\Delta a = 0$ to $\Delta a = 400\ \mu$m the value of J_R increases by a factor around 2.4 for $T = 0$, whereas J_R increases by a factor around 4.2 for $T/\sigma_Y = -0.75$. It is noted that J_R increasing by a factor 2.4 corresponds to K_R increasing by a factor 1.55.

4. DISCUSSION

From a qualitative standpoint, the present embedded process-zone model captures the effect of the T-stress quite realistically, reflecting its potential applicability to deal with the important effects of constraint, or loss thereof, in ductile fracture. We believe that models such as the present one have considerable promise as predictive tools for non-linear fracture mechanics analysis. In principle, there is no barrier to using such models in large-scale yielding situations with relatively large amounts of crack growth. There is no issue of identifying a crack-tip parameter to generalize T under large-scale yielding conditions; one simply computes the history of overall load, displacement and crack length given a separation law characterizing the fracture process of a given material. There is also no intrinsic difference in dealing with crack growth initiation and continuing growth with this approach and, in particular, there is no problem identifying different crack-tip characterizing parameters for stationary and growing cracks. An approach of this kind does require extensive, relatively sophisticated numerical work using a finite element code, but this is true of essentially all methods under consideration for highly non-linear fracture applications. Many of the potential applications of non-linear fracture analysis are of sufficient importance that the cost of a computational study is not a prohibiting factor.

An approach to applying the embedded process zone model to a non-linear fracture problem might involve the following steps. The parameters characterizing the continuum plasticity properties such as σ_Y and N would obviously be chosen to fit tensile stress strain data for the material in question. The two main parameters characterizing the traction–separation relation in the present model are Γ_0 and $\hat{\sigma}$. These could be regarded as phenomenological parameters chosen to fit one set of crack growth data for the material. A straightforward scheme might identify Γ_0 with the initiation value of J (extrapolated back to zero crack advance) and might select $\hat{\sigma}$ such that the initial slope of the predicted resistance curve (i.e. the tearing modulus—see below) coincides with that of the resistance curve data. Alternatively, Γ_0 and $\hat{\sigma}$ might be chosen to give a best fit of the crack growth data. In either case, the fitting process would require an analysis of the reference specimen used to generate the resistance curve data with iteration on $\hat{\sigma}$. Then, assuming the traction–separation law is capable of representing the fracture process in a phenomenological sense, the model could be used to predict crack growth in the material under both large and small-scale yielding conditions and under various constraint situations.

The toughest steels, such as the pressure vessel steel tested by Hancock *et al.* (1991) which was mentioned above, have values of R_0 which are as large as a centimetre or more. Higher strength, more brittle steels have values of R_0 as small as a fraction of a millimetre. Thus, depending on the material, the resistance curves in Figs 3 and 4 indicate that steady-state toughness levels are attained after crack advances ranging from a fraction of a millimetre for the least tough steels to more than several centimetres for the toughest materials. Indeed, resistance curve data for the toughest pressure vessel steels show no sign of attaining steady-state with increases of J_R of a factor of ten above J_{I^c} (equivalently, increases of K_R a factor of about three above K_{I^c}), corresponding to crack advances on the order of 1 cm [e.g. Vassilaros *et al.* (1980)].

It is of interest to make contact with the non-dimensional tearing modulus introduced by Paris *et al.* (1979) to measure the initial slope of the crack growth resistance curve. Here, to avoid confusion with the T-stress, the tearing modulus will be denoted by T_R. Its definition is

$$T_R = \frac{E}{\sigma_Y^2}\left[\frac{\mathrm{d}J_R}{\mathrm{d}\Delta a}\right]_{\Delta a=0}. \tag{8}$$

When expressed in terms of the small-scale yielding variables of the present study and put into the relevant non-dimensional form, the tearing modulus becomes

$$T_R = 3\pi(1-\nu^2)\left[\frac{\mathrm{d}(\Gamma_R/\Gamma_0)}{\mathrm{d}(\Delta a/R_0)}\right]_{\Delta a=0} = 6\pi(1-\nu^2)\left[\frac{\mathrm{d}(K_R/K_0)}{\mathrm{d}(\Delta a/R_0)}\right]_{\Delta a=0}. \tag{9}$$

By virtue of the discussion given earlier, one sees that computed values of the non-dimensional tearing modulus using the embedded process zone model will depend primarily on $\hat{\sigma}/\sigma_Y$ (and N). Thus, this quantity may be a particularly appropriate one to use in the process of identifying $\hat{\sigma}$ to fit a particular set of resistance curve data. Data presented by Paris *et al.* (1979) for a wide range of metals show that the tearing modulus tends to scale with toughness, with the most brittle metals having values of T_R on the order of unity and the toughest steels having values as large as several hundreds. The largest meaningful value of T_R predicted by the present model for a solid with a strain exponent of $N = 0.1$ is about 100 [cf. Fig. 3 of Tvergaard and Hutchinson (1992)]. These largest predicted values are somewhat less, by about a factor of two, than the values of T_R measured for the toughest steels, such as the nuclear pressure vessel steel A533B and the steel tested by Hancock *et al.* (1991) (ASTM 719 grade A). For reasons discussed below, we do not believe that the present model, without some modification, can be applied to these toughest materials.

Figure 7, which is drawn from results in Tvergaard and Hutchinson (1992), shows the computed steady-state toughness and the extent l_{ss} of the steady-state fracture process zone ahead of the tip as a function of $\hat{\sigma}/\sigma_Y$ for two levels of strain hardening and for the nominally high triaxiality case $T = 0$. (The steel tested by Hancock *et al.* has $N = 0.1$.) For $N = 0.1$, the steady-state toughness becomes very large as $\hat{\sigma}/\sigma_Y$ approaches a value between 3.75 and 4.0; the corresponding value of $\hat{\sigma}/\sigma_Y$ for $N = 0.2$ lies between 5.0 and 5.5. Note that the size of the steady-state fracture process zone becomes smaller and smaller relative to R_0 as these same values are approached. The legitimacy of a model based on a traction–separation law specified on a line breaks down when l_{ss} becomes too small. For a fracture process involving void nucleation, growth and coalescence, Tvergaard and Hutchinson found that there are two regimes of behaviour: (i) l_{ss} is large compared to the void spacing so that the present line model of the process zone is applicable and (ii) l_{ss} becomes on the order of the void spacing and the line model must give way to a picture involving interaction between the tip and one or two discrete voids ahead of it. The second regime is in effect when $\hat{\sigma}/\sigma_Y$ approaches the values listed above. Very tough materials such as the pressure vessel steels appear to fall into this second regime. It is not clear whether some modification of the present line model could be used in this regime—the incorporation of some strain dependence to model the effect of straining on void nucleation, for example. The challenge is to come up

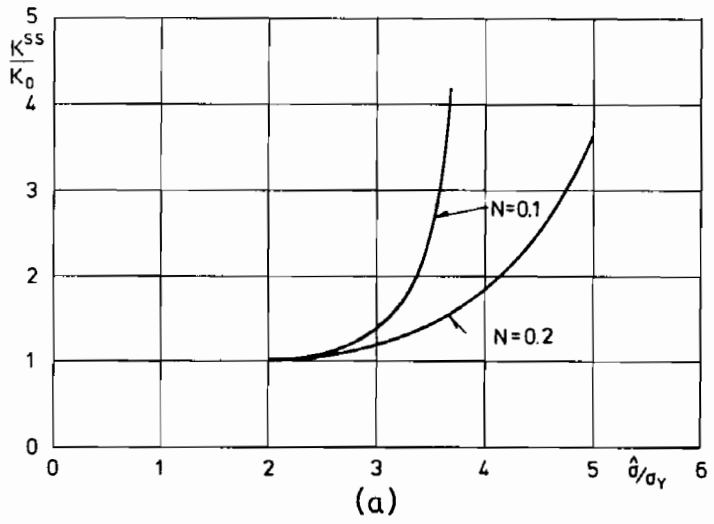

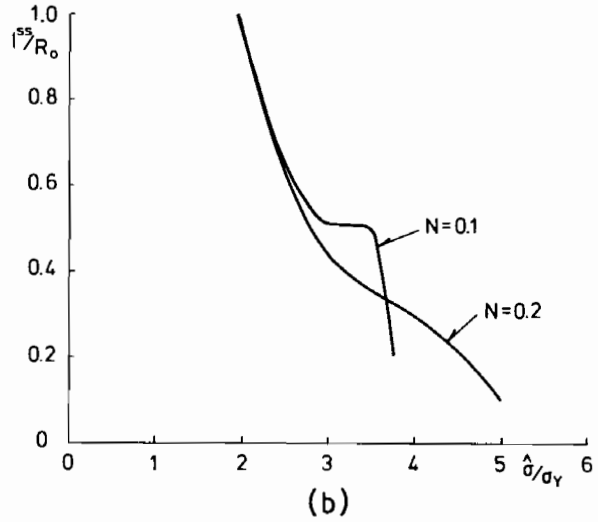

Fig. 7. Steady-state toughness and length of the fracture process zone as functions of $\hat{\sigma}/\sigma_Y$, for $T/\sigma_Y = 0$ and $\sigma_Y/E = 0.003$. (a) Toughness. (b) Length of the fracture process zone. [From Tvergaard and Hutchinson (1992).]

with a model of the fracture process which could be embedded within the elastic–plastic continuum so that crack initiation and growth could be computed for these very tough materials.

Acknowledgement—The work of J.W.H. was supported in part by the National Science Foundation under Grant NSF-MSS-92-02141 and by the Division of Applied Sciences, Harvard University.

REFERENCES

Betegon, C. and Hancock, J. W. (1991). Two-parameter characterization of elastic–plastic crack-tip fields. *J. Appl. Mech.* **113,** 104–110.

Du, Z.-Z. and Hancock, J. W. (1991). The effect of non-singular stresses on crack-tip constraint. *J. Mech. Phys. Solids* **39,** 555–567.

Hancock, J. W., Reuter, W. G. and Parks, D. M. (1991). Constraint and toughness parameterised by *T*. *ASTM Symposium on Constraint Effects in Fracture*, Indianapolis.

Hutchinson, J. W. (1973). Finite strain analysis of elastic–plastic solids and structures. In *Numerical Solution of Nonlinear Structural Problems* (Edited by R. F. Hartung), p. 17. American Society for Mechanical Engineers, New York.

Larsson, S. G. and Carlsson, A. J. (1973). Influence of non-singular stress terms and specimen geometry on small-scale yielding at crack tips in an elastic–plastic material. *J. Mech. Phys. Solids* **21,** 263–277.

O'Dowd, N. P. and Shih, C. F. (1991). Family of crack-tip fields characterized by a triaxiality parameter—I. Structure of fields. *J. Mech. Phys. Solids* **39,** 989–1015.

O'Dowd, N. P. and Shih, C. F. (1992). Family of crack-tip fields characterized by a triaxiality parameter—II. Fracture applications. *J. Mech. Phys. Solids* **40,** 939–963.

Paris, P. C., Tada, H., Zahoor, A. and Ernst, H. (1979). The theory of instability of the tearing mode of elastic–plastic crack growth. In *Elastic–Plastic Fracture* (Edited by J. D. Landes *et al.*), pp. 5–36. ASTM STP 668, American Society of Testing Materials.

Rice, J. R. (1974). Limitations to the small scale yielding approximation for crack tip plasticity. *J. Mech. Phys. Solids* **22,** 17–26.

Tvergaard, V. (1990). Effect of fibre debonding in a whisker-reinforced metal. *Materials Science and Engineering* **A125,** 203–213.

Tvergaard, V. and Hutchinson, J. W. (1992). The relation between crack growth resistance and fracture process parameters in elastic–plastic solids. *J. Mech. Phys. Solids* **40,** 1377–1397.

Tvergaard, V. and Hutchinson, J. W. (1993). The influence of plasticity on mixed mode interface toughness. *J. Mech. Phys. Solids* **41,** 1119–1135.

Vassilaros, M. G., Joyce, J. A. and Gudas, J. P. (1980). Effects of specimen geometry on the J–R curve for ASTM A533B steel. In *Fracture Mechanics: Twelfth Conference*, ASTM STP 700, pp. 251–270. American Society of Testing Materials.